# Alma Mater Studiorum Università di Bologna
# Archivio istituzionale della ricerca

Hierarchical chitinous matrices byssus-inspired with mechanical properties tunable by Fe(III) and oxidation

04 May 2024

# Hierarchical Chitinous Matrices Byssus-Inspired with Mechanical Properties Tunable by Fe(III) and Oxidation

*Devis Montroni*\*,1, *Marco Palanca*2, *Kavin Morellato*2, *Simona Fermani*1, *Luca Cristofolini*\*,2 *and Giuseppe Falini*\*,1

1 Department of Chemistry "Giacomo Ciamician", Alma Mater Studiorum − University of Bologna, via F. Selmi 2, 40126 Bologna, Italy.

2 Department of Industrial Engineering, Alma Mater Studiorum – University of Bologna, via Terracini 34, 40131 Bologna, Italy.

ABSTRACT: In this study the multi-scale hierarchical structure of the β-chitin matrix from the squid pen of *Loligo vulgaris* was used as substrate to prepare new bio-inspired materials. Finding inspiration from the byssus, aiming to mimic its peculiar mechanical properties, we chemically functionalized the β-chitin matrix with catechols, one of the main functional groups of the byssus. The obtained matrix preserved its multi-scale structural organization and was able to chelate reversibly Fe(III). Thus, it behaved as the byssus, acting as a metal cross-linkable matrix that upon metalation increased its Young's modulus, E (> 10 times). The functionalized matrix was also cross-linked by oxidation provoking an increase of the E (> 10 times) and first failure stress (> 5 times). The oxidation of the functionalized matrix followed by metalation slightly increased the material mechanical properties. In conclusion, we showed that specific bio-inspired functionalities can be added in a multi-scale and natural matrix tuning its mechanical properties without altering its overall organization.

Keywords: chitin; catechols; metal ions; hierarchical structures; bioinspired

\*Corresponding authors. E-mail:     giuseppe.falini@unibo.it (G. Falini)

devis.montroni2@unibo.it (D. Montroni)

luca.cristofolini@unibo.it (L. Cristofolini)

## 1. INTRODUCTION

Nature is able to produce materials with a multi-scale ordered hierarchical structure. Those materials can be organic (mostly polymeric), inorganic, or organic-inorganic composites.(Eder, Amini, & Fratzl, 2018; Holland, Blanford, Do, & Stein, 1999; Meyers et al., 2006; Seto et al., 2012) In them an ordered hierarchical structure provides functional advantages compared to unstructured or disordered materials, such as mechanical properties and biocompatibility.(Kennedy et al., 1999)

Chitin, poly-(β-(1–4)-N-acetyl-D-glucosamine), is the most abundant biopolymer in the animal kingdom. It is also widely diffused among all the known species (being present in over 70 % of them), making it the most common polymeric material used by nature.(Fernandez & Ingber, 2013; Montroni, Fermani, et al., 2019; Montroni, Marzec, Valle, Nudelman, & Falini, 2019; Muzzarelli, 2013) It is present in a huge variety of hierarchical organizations aimed to different purposes, being the most common for protective or structural functions.(Al-Sawalmih et al., 2008; Ehrlich et al., 2010; Montroni, et al., 2019; Weaver et al., 2012; Yang et al., 2019) Some examples of structured chitinous materials are found in sponges, where they occur as nanostructured micro-porous skeletal elements.(Shaala et al., 2019; Wysokowski et al., 2015) In many butterflies, such as the *Morpho* genus, chitin-based wings exhibit a photonic behaviour due to their periodic structure.(Ghiradella & Radigan 1994; Kinoshita, Yoshika, Fujii, & Okamoto, 2002) In the squid pen of *Loligo vulgaris* a hierarchical self-similar structure with micro-fibers of different size, composed themselves of crystalline nano-fibrils, is observed and it is oriented along the long axis of the pen. Those fibers compose different layers that overlap forming the squid pen.(Hunt & El Sherief, 1990)

Chitin has been widely applied in material science, drug delivery, medicine, optic, water remediation, etc.(Anitha et al., 2014; Chabbi et al., 2020; Dev et al., 2010; Shams, Ifuku, Nogi, Oku, & Yano, 2011; K. Zhu et al., 2019) This variety of fields of application is due to chitin's multi-properties, among which mechanical resistance, biodegradability, biocompatibility, transparency, etc.(Pillai, Paul, & Sharma, 2009; Ravi Kumar, 2000; Singh, Dutta, Kumar, Kureel, & Rai, 2018; Tsai, Payne, & Shen, 2018) Chitin is frequently utilized in its deacetylated form, named chitosan when the chitin's degree of acetylation (DA) is lower than 35 %.(Pillai et al., 2009) Chitin is hardly soluble only in some strong polar organic solvents, while chitosan is easily solubilized in acid solutions.(Ravi Kumar, 2000) Moreover, chitin has better mechanical properties than chitosan, especially in the wet state, and a higher tendency to self-assemble in fibers.(Harmoudi et al., 2014; Ifuku et al., 2013; Rathke & Hudson, 1994)

Nature's huge pool of efficient and performing materials has stimulated different bioinspired synthetic approaches to emulate them. The synthesis of those new materials when performed by the bottom-up approach fails in obtaining multiscale hierarchical ordered structures, as those produced by nature. An alternative approach is using a natural material, in which the hierarchical structure is preserved at a defined scale, and adding one or more levels of complexity. This approach allows combining the properties of the

two levels of complexity in a new functional material.(Ianiro et al., 2014) From the chemical point of view, the easiest way to add a property to a hierarchical material, as a polymeric one, is by functionalization with a chemical moiety. The wide application of chitinous materials has stimulated the development of different chemical routes to modify their properties.(Kurita, 2001; Sashiwa & Aiba, 2004) However, in these studies chitosan was mainly involved, even if reported as chitin.(Macquarrie & Hardy, 2005; Martin et al., 2002; Mi, Shyu, Chen, & Lai, 2002)

Among chemical functional groups, catechols have been widely used to obtain materials with high mechanical and adhesive properties, especially in wet environments.(J. Chen et al., 2020; Filippidi et al., 2017) This functionalization has been inspired by the studies on the byssus, the proteic thread produced by mussels to anchor to a substrate and resist to currents and waves. It presents catechol moieties, as 3,4-dihydroxyphenylalanine (DOPA), that are responsible for the thread's mechanical, self-healing, and adhesive properties.(Harrington, Masic, Holten-andersen, Waite, & Fratzl, 2010; Hwang et al., 2012; Montroni et al., 2018; Nicklisch & Waite, 2012)

Two catechol's chemical properties have stimulated its utilization in material sciences: i) the ability to chelate in reversible way transition metal ions as a bidentate ligand, and ii) the ability to cross-link covalently by the Michael addition reducing back to its dihydroxy state, upon oxidation to quinone.(Asghari et al., 2015; Guo, Ni, Wei, & Ren, 2015; L. Li, Smitthipong, & Zeng, 2015; Y. Li, Wen, Qin, Cao, & Wang, 2017; Qiao et al., 2014; H. Xu et al., 2012; Z. Xu, 2013) The catechol functionalization has been observed to increase the mucoadhesive property of materials.(Kim, Kim, Hyun, & Lee, 2015; L. Li et al., 2015; J. Xu, Strandman, Zhu, Barralet, & Cerruti, 2015) Chitosan functionalized with catechols produced a biocompatible mucoadhesive patch that was studied as drug delivery system.( Xu et al. 2015 ) Qiao at al. 2014, developed a solution of catechol-derived chitosan and Fe(III) that formed a gel upon an increment of pH.(Qiao et al., 2014) This material was studied as drug delivery system for Doxorubicin. Kim et al. 2015 tested the mucoadhesion capability of a chitin-catechol polymeric film defining it as "the most potent mucoadhesion polymers reported to date".(Kim et al., 2015) A catechol-chitosan coating was also applied to prevent oxidative stress to interfere with bone implant healing process.(W. Chen et al., 2017) Catechol-chitosan polymers were applied by Ryu et al. 2014 as a material self-converting in water insoluble dehydrated film, with application in food packaging.(Ryu, Jo, Koh, & Lee, 2014) Moreover, the metal-chelating ability of catechol-based matrices have also been exploited in water remediation.(Montroni et al., 2017) Most importantly, this chelating ability is also responsible for the self-healing properties of the byssus. In fact, along with traction the catechol-metal bond acts as sacrificial bond, avoiding initial critical damages, to reform after the stress is removed. Following this knowledge in 2017, Filippidi et al. developed a byssus inspired hydrogel exhibiting self-healing properties. (Filippidi et al., 2017)

The aim of our study is to modify chemically the hierarchically organized natural chitin matrix from the pen of the squid *L. vulgaris*, increasing its complexity by functionalization with catechols. This material is actually a good candidate for this synthetic approach. In fact, when an alkaline treatment at high temperatures is used it can induce up to 45 % of deacetylation, producing glucosamine units, with minimal changes in morphology and structure of the scaffold.(Montroni, Fermani, et al., 2019; Montroni, Sparla, Fermani, & Falini, 2020) Those amino groups are supposed to be mainly located in amorphous regions or in the external surface of the fibrils, and represent a perfect target for a coupling reaction. The final goal of this study is to obtain a structured material at which the functional properties of catechols can be added, as occurs in the byssus. The hypothesis is that the chemical functionalization will allow the control of the mechanical properties upon reversible chelation of Fe(III), or by covalent cross-linking by oxidation.

## 2. EXPERIMENTAL SECTION

*2.1 Materials:* All reagents and solvents were purchased from Sigma Aldrich and utilized without any further purification. Squid pens from *Loligo vulgaris* were collected from a local market. Once hydrated, the lateral blades were isolated, cleaned with abundant distilled water (carefully eliminating eventual residual tissues) and ethanol 70 vol.%, cleaned again using distilled water, and then stored dry in a desiccator.

*2.2 Synthesis of the matrices:* The squid pen was initially deproteinized inserting 2.5 g of squid pens, previously washed as described, in 100 mL of a boiling 1 M NaOH solution and stirring gently for 1 h.(Ianiro et al., 2014; Montroni et al., 2020) After that, the solution was changed with a fresh 1 M NaOH solution and refluxed for 1 h. The obtained chitin films were washed at room temperature first with a 1 M NaOH solution and then with distilled water until the washing solution had neutral pH. The films were stored dry in a desiccator.

The chitin was successively deacetylated by adding 400 mg of the deproteinized chitin in 20 mL of a 5 M NaOH boiling solution for 2 h under a gentle stirring.(Montroni, et al., 2019)  The obtained chitin was then washed at room temperature first with a 5 M NaOH solution and then with distilled water until washing solution had neutral pH. The deacetylated chitin (DC) was stored dry in a desiccator.

The DC (800 mg) was then soaked in 90 mL of a pH 4.0 HCl solution for 15 minutes. In 45 mL of a 1:1 mixture of ethanol and water, acidified to pH 4.0, 466 mg (2.5 eq. respect to the deacetylated glucosamine units) of 1-ethyl-3-(3-dimethylaminopropyl)carbodiimide and 266 mg (1.5 eq. respect to the deacetylated glucosamine units) of 3,4-dihydroxyhydrocinnamic acid were solubilized and stirred for one minute.(Kim et al., 2015; Qiao et al., 2014; Ryu et al., 2011; Zvarec, Purushotham, Masic, Ramanujan, & Miserez, 2013) The ethanol/water solution was slowly dropped on the former one under stirring. The reaction mixture was set

132  on a rocking table in a dark room at 25 °C for 24 h. The catechol-functionalized deacetylated chitin matrices

133  ($C_f$-DC) were washed soaking them three times in an HCl pH 4.0 solution for 10 minutes. The matrices were

134  conserved wet in the pH 4.0 solution at 4 °C in the dark.

135  The crosslinking of the $C_f$-DC was induced soaking the previously prepared matrices in 200 mL of a carbonate

136  buffer 50 mM pH 9.5 for 24 h on a rocking table.(H. Lee, Dellatore, Miller, & Messersmith, 2007) The cross-

137  linked $C_f$-DC (C$C_f$-DC), were conserved in water at 4 °C in the dark.

138  The metal insertion in the matrices was performed using a 10 mM bicine buffer at pH 7 containing $FeCl_3$ or

139  $VCl_3$ in a 1:3 ratio between the deacetylated units and the metal ions.(Filippidi et al., 2017) The appropriate

140  amount of matrices were then soaked in the metal solution to get a 10 mg·mL$^{-1}$ dispersion of matrix in the

141  solution and set on a rocking table for 30 minutes. The specimens were then washed four times in water,

142  soaking the specimens for 5 minutes each time. The specimens were conserved in water at 4 °C in the dark.

143  The metal removal was performed soaking 10 mg·mL$^{-1}$ of sample in an EDTA 10 mM solution and setting the

144  solution on a rocking table for 30 minutes. The specimens were then washed four times in PremilliQ water,

145  soaking the specimens for 5 minutes each time, and conserved in PremilliQ water at 4 °C in the dark.

146  *2.3 Determination of the degree of acetylation:* The degree of acetylation (DA) of chitin was determined using

147  solid-state nuclear magnetic resonance (NMR). The NMR experiments were performed on a Bruker Advance

148  spectrometer operating at the frequency of 300 MHz for proton (equipped with a 4 mm MAS BB probe) using

149  the combined techniques of cross-polarization and magic angle spinning. Field strengths corresponding to

150  90° pulses of 4.5 μs were used for the matched spinlock cross-polarization transfer $^1$H to $^{13}$C. The contact

151  time was 1 ms, and the recycle delay 10 s. A typical number of 500–3000 scans were acquired for each

152  spectrum. The chemical shifts were externally referred by setting the carbonyl resonance of glycine to 176.03

153  ppm. Glycine full width at half-height better than 27 Hz. The spinning speed was set at 8000 Hz for all

154  specimens. The assignment of NMR signals and the DA calculation was done according to literature.(Heux,

155  Brugnerotto, Desbriéres, Versali, & Rinaudo, 2000)

156  *2.4 Swelling measurement:* The measure of the chitin specimen swelling in water was carried out first

157  weighting a dry specimen, conserved overnight in a desiccator under vacuum, and secondly weighting it after

158  soaking in water overnight, prior blotting it on a paper towel. The measures at pH 4 were performed using

159  an HCl solution at pH 4.0. Mass measurements were performed using a Sartorius CP225D (± 0.01 mg) on at

160  least 50 mg of initial dry specimen. The swelling measurements were performed at least on three

161  independent specimens.

162  *2.5 Spectroscopic analysis:* UV-Vis spectra were collected in transmission acquiring between 240 and 800 nm

163  with a 1 nm resolution, and an average time of 0.1 s using a Varian Cary 300 Bio spectrophotometer.

Raman spectra were acquired using a Renishaw Raman Invia spectrophotometer interfaced with a Leica DMLM optical microscope. The spectrophotometer was equipped with a diode laser (780.0 nm, $P_{max}$ = 300 mW), an edge filter to remove the Rayleigh scattering, a monochromator (1200 lines·$mm^{-1}$), and a CCD detector. The instrument was calibrated using a silicon wafer (520 $cm^{-1}$). The spectra were acquired summing three spectra using a 1 % power and 10 s of acquisition.

*2.6 Synchrotron X-ray diffraction:* X-ray fiber diffraction diagrams were collected at XRD1 beamline, Elettra, Trieste, Italy. Each frame was collected at the peak wavelength (0.9999 Å) using an exposure of 60 s. The X-ray diffraction diagrams were analysed using Fit2D software.

*2.7 Scanning electron microscopy:* SEM images were acquired with a Philips SEM 515 using 15 eV. The wet specimens were lyophilized, eventually cut with a scalpel to expose the section, glued on carbon tape, dried overnight in a desiccator, and coated with 20 nm of gold prior to image them.

*2.8 Uniaxial tensile test:* Each specimen was cut in a proper dimension using scissors before the de-proteination, maintained hydrated after the synthesis and tested hydrated. The actual width and thickness of each hydrated specimen were measured after the synthesis using a SM-LUX POL microscope collecting images with a 5.0 MP digital camera (Motic Moticam 5+). The images were analysed using ImageJ. Each specimen was about 60 mm long, 5 mm wide, and 0.15-0.30 mm thick (the thickness varied between specimens, because of the intrinsic variability of the initial biological specimens). Monotonic uniaxial tensile tests were performed using a universal testing machine (Mod. 8032 with 8800 controller, Instron, UK) and dedicated grips, leaving a free length of about 50 mm between the clamps. The tests were performed at room temperature imposing a strain rate of 0.33 %·$sec^{-1}$ to all specimens (this resulted in an actuator speed of the order of 10 mm·$min^{-1}$, depending on the actual gauge length of each specimen). As the curves were rather linear until failure started, the following parameters could be calculated, taking into account the actual dimensions of each specimen:

- The Young's modulus (E), defined as the slope of the linear part of the stress-strain curve;

- The stress ($\sigma_{1st\ failure}$) and strain ($\varepsilon_{1st\ failure}$) when specimen failure started (yield, detected as a drop of the force by 1 %);

- The maximum stress ($\sigma_{max}$);

- The work per unit volume required to reach yield ($Work_{1st\ failure}$) in J·$mm^{-3}$.

All specimens failed in one of the two ways: either abrupt fracture, perpendicular to the specimen's axis, or progressive unravelling of the fibers. The two modes of failure were not associated with specific specimen groups. To this reason, the maximum elongation and the total work per unit volume were not evaluated because they were not robust indicators of the specimens' behaviour. At least five specimens were tested

196  for each group. The Peirce criterion was adopted to detect and exclude outliers (15 % of the data had to be

197  excluded).(Ross, 2003) Normality was checked for each treatment group (sample) with the Kolmogorov-

198  Smirnov test. As the data did not follow a normal distribution, non- parametric statistical tests were applied

199  to each calculated mechanical parameters: Kruskal-Wallis test followed by a Dunn's post hoc.

200

201  3. RESULTS

202  In this work the chitinous hierarchical structure of the squid pen of *L. vulgaris* was functionalized on the free

203  amino groups with catechols and then treated with Fe(III) and/or oxidized. A schematic of the different

204  matrices produced is reported in Figure S1.

205  The squid pen from *L. vulgaris* is a chitin based matrix composed of 40-50 wt.% of proteins.(Montroni et al.,

206  2019) The proteins were removed from the matrix using an aqueous 1 M NaOH solution treatment under

207  reflux for 2 h. This occurs without inducing any change in the morphology and structure of the chitinous

208  matrix in the pen. (Montroni, Fermani, et al., 2019; Montroni et al., 2020) After this first alkaline treatment,

209  the DA of chitin was about 88 %.(Montroni et al., 2019). A second alkaline treatment was performed using a

210  5 M NaOH solution under reflux for different times, see Figure 1 step 1, to increase the number of free amino

211  moieties in the matrix.(Montroni et al., 2019). The treatment was performed for 2 h, 8 h, or 24 h obtaining a

212  DA of $76.9 \pm 0.6$ %, $56 \pm 1$ %, and $32 \pm 1$ %, respectively (Figure S2). The 24 h treated chitosan matrix appeared

213  curly and not uniform, and was not used for further experiments. The two deacetylated chitin (DC) samples

214  had water swelling higher than 200 wt.%, Table S1, that was reached in less than 15 minutes.  The second

215  step of the synthesis was the insertion of the catechol group, Figure 1 step 2. The reaction was performed by

216  applying a standard peptide coupling in water. The synthesis was optimized in pH and time as reported in the

217  SI (Figure S3). After this synthetic step, the catechol-functionalized DC ($C_f$-DC) obtained from the chitin

218  deacetylated for 8 h was in a gel state with swelling of $3000 \pm 700$ %, Table S1. Despite the birefringence of

219  the matrix appeared conserved, it was impossible to perform uniaxial tensile tests on this set of specimens

220  due to difficulties in handling, even after Fe(III) treatment or crosslinking. Thus, the successive experiments

221  were performed only using the $C_f$-DC obtained from the chitin deacetylated for 2 h.

222
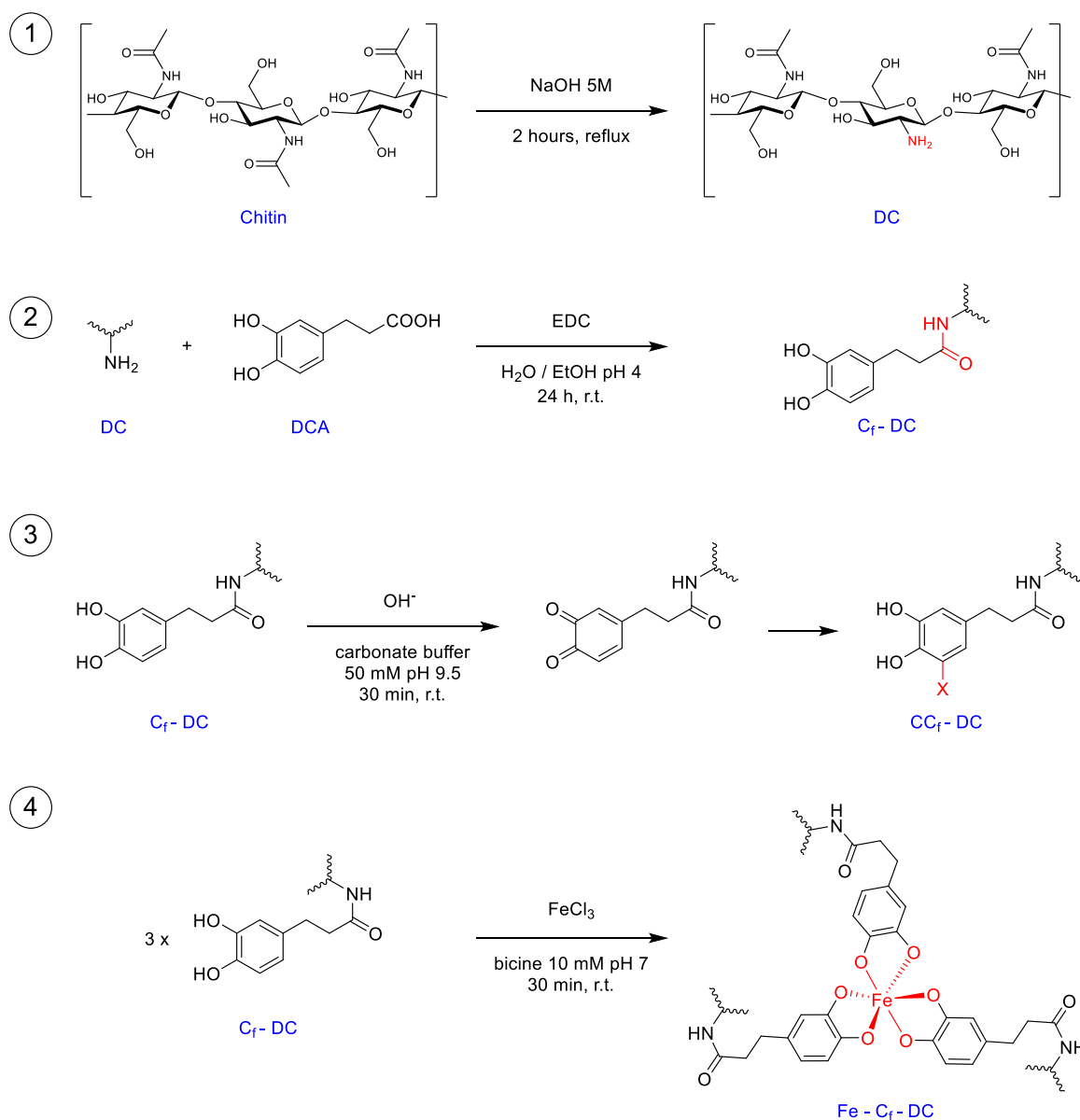
**Figure 1.** Scheme of the synthetic steps to functionalize the matrix. 1) Chitin partial de-acetylation, to obtain the DC. 2) DC functionalization with catechols, to obtain the $C_f$-DC. 3) $C_f$-DC basic crosslinking, to obtain the $CC_f$-DC, where X can represents a heteroatom (such as oxygen from –OH groups, or nitrogen from –$NH_2$ groups) or another aromatic ring. 4) Metal insertion in the $C_f$-DC, to obtain Fe-$C_f$-DC.

The Fe(III) chelation in the $C_f$-DC was optimized testing different pHs of bicine buffer, as reported in Figure S4. UV-Vis spectra of the $C_f$-DC before and after Fe(III) insertion showed a typical broad catechol–iron peak appearing between 500 and 700 nm in the metal treated matrices.(Guo et al., 2015) This peak came along with a shift of the catechol signal from 280 to 288 nm. Only a weak signal of the o-quinone (oxidized catechol) at 400 nm was observed.(Guo et al., 2015) After Fe(III) insertion, the matrix appeared of a bright blue (Figure 2).

DC    C$_f$-DC    Fe-C$_f$-DC    CC$_f$-DC    Fe-CC$_f$-DC    V-CC$_f$-DC

EDTA →    EDTA →    EDTA →

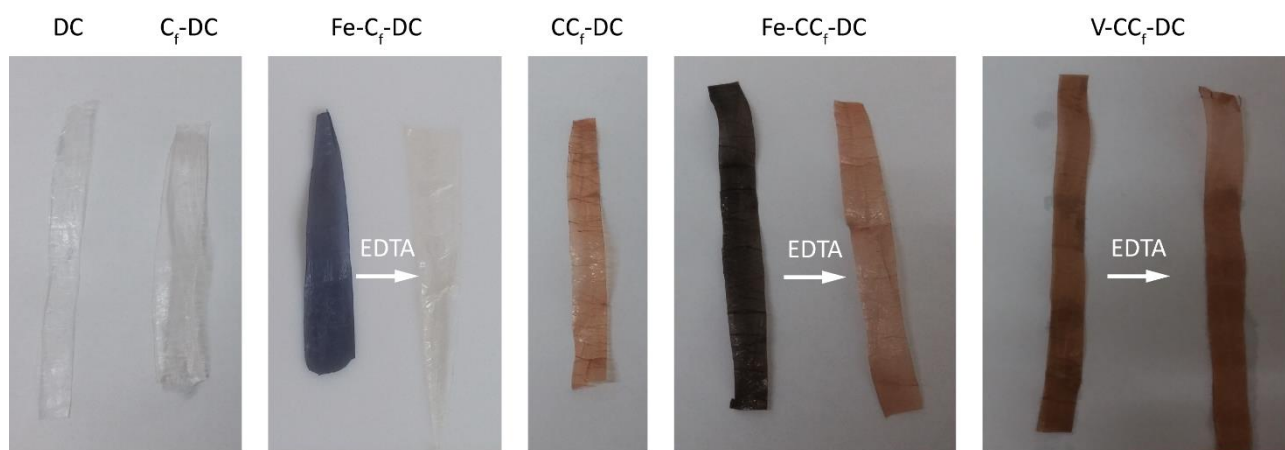**Figure 2.** Picture of the different matrices obtained in the different stages of the synthesis. Scale bar 5 mm.

The coloration disappeared after treatment with EDTA and the UV-Vis spectrum restored as in the C$_f$-DC. The presence of catechol-iron(III) complexes was also confirmed using Raman spectroscopy, Figure 3.(Guo et al., 2015) No significant change in the swelling was observed after metal insertion, Table S1.
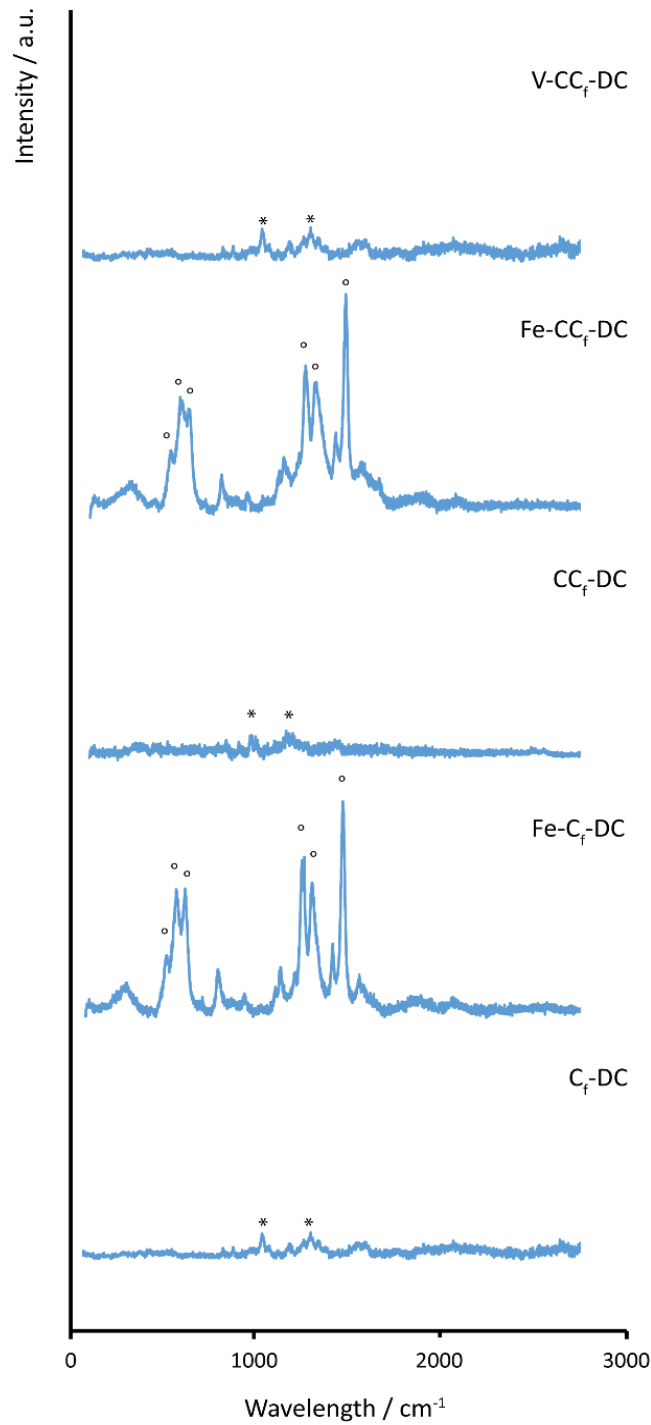
**Figure 3**. Raman spectra of the different matrices. According to literature, all the samples containing iron show only catechol-Fe signals (°), as the Fe-O bond vibrations in the 500–700 $cm^{-1}$.(Guo et al., 2015) Chitin signals (*) were observed in all the samples.(Kaya et al., 2017)

The mechanical properties were evaluated for each sample group (Table 1, Figure 4). In particular, the $C_f$-DC showed, in comparison with the DC, lower first failure ($\sigma_{1st\ failure}$), maximum stress ($\sigma_{max}$), work and Young's

249 modulus (E), and higher first failure elongation ($\varepsilon_{1st\ failure}$). The Fe-$C_f$-DC showed, with respect to $C_f$-DC, an

250 increase of the $\sigma_{1st\ failure}$ and of the $\sigma_{max}$ (not statistically significant), and at the same time a significant

251 decrease of $\varepsilon_{1st\ failure}$, with a consequent higher E (> 10 times), both comparable with the DC.

252 Catechols can also undergo covalent crosslinking by oxidation, Figure 1, step 3. The $C_f$-DC was covalently

253 cross-linked using a basic environment as an alternative way to tune its mechanical properties. A basic

254 environment was chosen instead of stronger oxidative conditions to get a slow oxidation that would allow

255 the matrix to physically reorganize its structure along the reaction. Moreover, this slower process would help,

256 avoiding as much as possible, to re-oxidize the catechols after the cross-linking. Three different pHs were

257 tested, pH 7, 9.5 and 14, for two different times, 24 h and 48 h. The best mechanical parameter results were

258 obtained using the pH 9.5 for 24 h, which showed a higher $\sigma_{max}$ and E, and a lower swelling (300 ± 100 %),

259 diagnostic for a proper cross-linking, compared to the other conditions (see SI for more details). The values

260 were comparable with those of DC. If compared to the $C_f$-DC an increment of more than 10 times in E, 3 times

261 in the work, and over 5 times in the $\sigma_{1st\ failure}$ and $\sigma_{max}$ were observed.

262

263
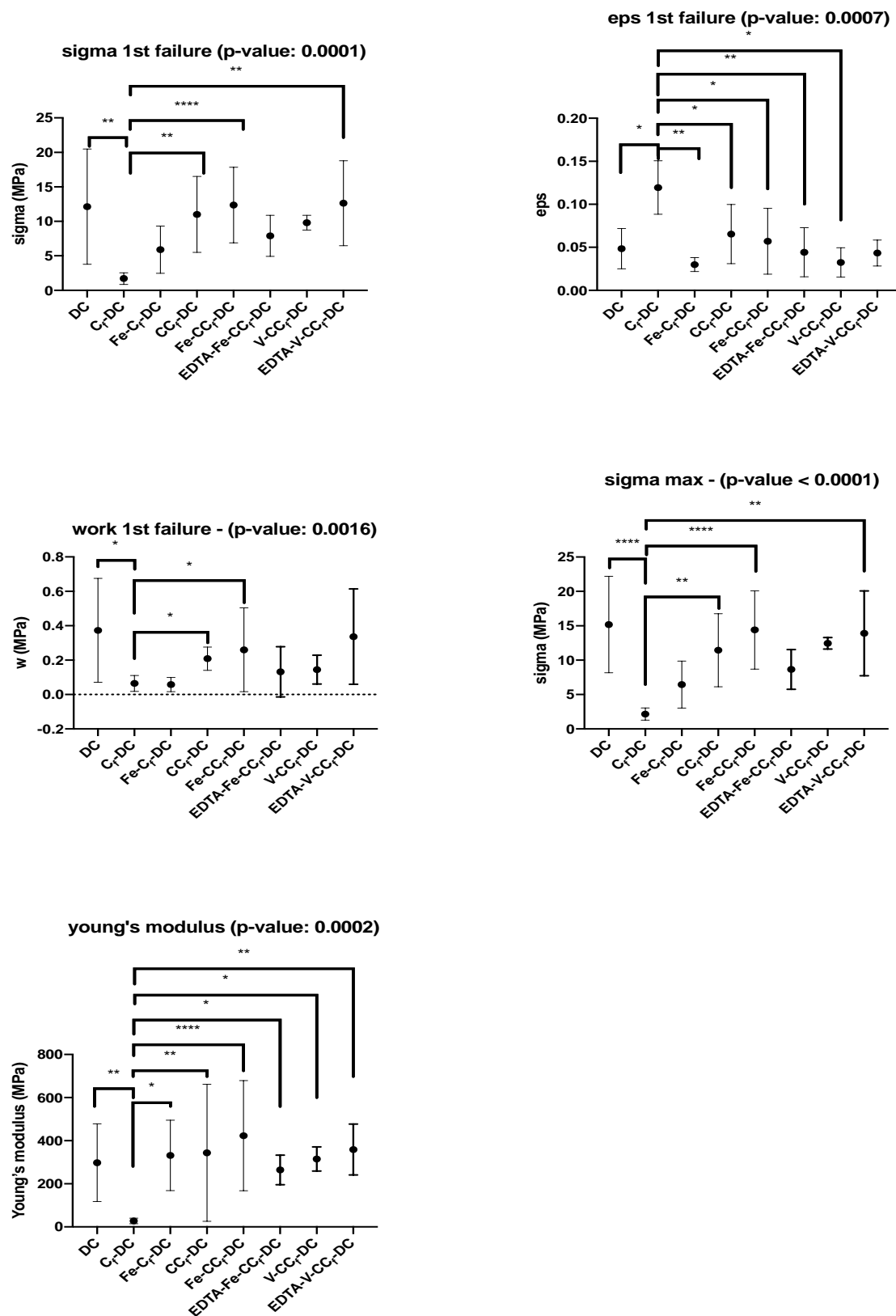
**Figure 4.** Mechanical data of the different matrices synthetized. For each mechanical data the overall significance of the Kruskal-Wallis test is reported. The level of Dunn's post-hoc statistical significance is reported between groups. \*\*\*\*: p-value < 0.0001; \*\*\*: p value < 0.001; \*\*: p-value < 0.01; \* = p-value < 0.05.

268

**Table 1.** Mechanical parameters of the matrices synthetized.

| Sample | $\sigma_{1st\ Failure}$ (MPa) | $\varepsilon_{1st\ Failure}$ | Work$_{1st\ Failure}$ (MPa) | $\sigma_{max}$ (MPa) | E (MPa) |
|---|---|---|---|---|---|
| DC | 12 ± 8 | 0.07 ± 0.02 | 0.4 ± 0.3 | 15 ± 7 | 300 ± 100 |
| C$_f$-DC | 1.7 ± 0.8 | 0.12 ± 0.03 | 0.06 ± 0.04 | 2.2 ± 0.8 | 30 ± 10 |
| Fe-C$_f$-DC | 6 ± 3 | 0.03 ± 0.01 | 0.06 ± 0.04 | 7 ± 3 | 300 ± 200 |
| CC$_f$-DC | 11 ± 5 | 0.07 ± 0.03 | 0.21 ± 0.06 | 12 ± 5 | 300 ± 300 |
| Fe-CC$_f$-DC | 12 ± 5 | 0.06 ± 0.04 | 0.2 ± 0.2 | 14 ± 6 | 400 ± 200 |
| EDTA-Fe-CC$_f$-DC | 8 ± 3 | 0.05 ± 0.03 | 0.1 ± 0.2 | 9 ± 3 | 260 ± 60 |
| V-CC$_f$-DC | 10 ± 1 | 0.03 ± 0.02 | 0.15 ± 0.08 | 12.4 ± 0.8 | 320 ± 60 |
| EDTA-V-CC$_f$-DC | 13 ± 5 | 0.05 ± 0.02 | 0.4 ± 0.3 | 14 ± 4 | 360 ± 90 |

270

Successively, Fe(III) was inserted in the cross-linked matrices in a 3:1 molar ratio between the free amine groups and Fe(III) (Fe-CCf-DC), Figure 1 step 4. The UV-Vis absorption peak for catechol-Fe(III) complexes was observed and the Raman spectra showed signals of catechol-Fe(III) complexes (Figure 3 and S6). The Fe-CCf-DC was then treated using EDTA inducing a loss of the UV-Vis absorption band of the catechol-Fe complex and a change in the color, Figure 2.

The Fe-CCf-DC showed a slight improvement (about 20 %) of the E, $\sigma_{1st\ failure}$, $\sigma_{max}$, and Work, and an equal decrease in the $\varepsilon_{1st\ failure}$ compared to the CCf-DC, but all the differences between the two groups were not statistically significant. A decrease in the swelling to 260 ± 40 % was observed. Once treated with EDTA, the parameters became more similar to the ones of CCf-DC.

To test the effect of massive oxidation on the system in comparison to the metal coordination we exposed the CC$_f$-DC to V(III) that has a chelating ability similar to Fe(III), but that instead of complexation induces oxidation on the catechols. The matrix exposed to V(III) (V-CC$_f$-DC) showed a broad peak at about 550 nm (Figure S6) but no signals of the catechol-V(III) complex were detected using Raman spectroscopy (Figure 3).

The V-CC$_f$-DC showed similar mechanical properties to the CC$_f$-DC, despite a drop of the swelling to 230 ± 10 % occurred due to the further cross-linking of the matrix. Contrary to the Fe(III) treated sample, the V-CC$_f$-DC one when treated with EDTA did not change properties (Figure 4; Tables S1 and S2).

14

287    The overall structural integrity of the matrices was investigated by fiber XRD using synchrotron radiation,

288    Figure 5 and Table S2. The diffraction images showed how all specimens maintained a comparable fibril

289    alignment, evaluated by the azimuthal angular spread of the reflection (002), Table S2. Indeed, the full width

290    at half maximum along the angle ranged between 30° and 34°, without any evident trend. The diffracted

291    intensity changed among the samples, Table S2. This could be due to a diverse crystallinity among them,

292    which reflected the variability always present in biological samples. Those containing Fe(III) or vanadium ions

293    showed a higher diffracted intensity, probably due to the positive contribute of the metal ions to the

294    coherent scattering of the structure. A slight structural reorganization was observed in the inter-planar

295    distance associated to the reflection (010). When the strongest catechol oxidation was performed (V-CCf-DC

296    sample) this distance was maximum at 11.1 Å, while in the starting sample (DC) was 10.7 Å.

297
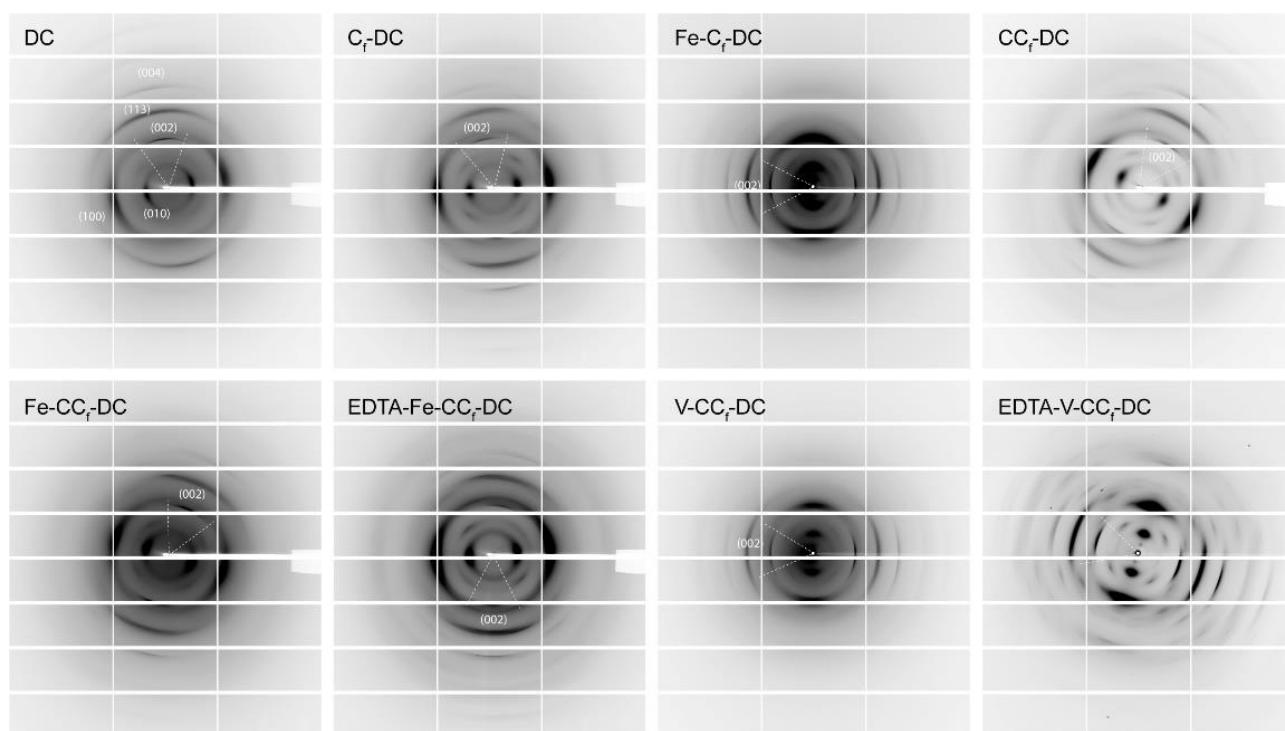


299    **Figure 5.** Synchrotron X-ray fiber diffraction images of the samples. In DC the Miller index of the reflection

300    are indicated. The diffraction peaks were indexed according to the monoclinic unit cell of β-chitin (Gardner,

301    & Blackwell, 1975). The dotted lines limit the angular spread of the reflection (002).

302

303    Interestingly, the presence of Fe(III) (Fe-$C_f$-DC) on the catechol functionalized chitin ($C_f$-DC) induced an

304    increase of the inter-planar distance from 10.5 Å to 10.9 Å.

305    The morphology and micro-structural organization of the specimens were examined using SEM, observing

306    the specimen's longitudinal section and external surface (Figure 6). The initial DC scaffold presented an

307    almost homogenous surface with a parallel fibrous organization and a lamellar structure in the section. As

15

308    reported in Montroni et al. 2019 and 2020, the alkaline treatment does not interfere with the chitinous

309    structure of the squid pen, therefore the DC is representative of the initial multi-scale structure of the pristine

310    pen.(Montroni, Fermani, et al., 2019; Montroni et al., 2020) A SEM image of a pristine squid pen is reported

311    in Figure S9. The specimen surface was almost unaltered in all specimens examined becoming a little more

312    homogenous compared to the DC but still showing an aligned fibrous arrangement. A difference in

313    morphology was observed in sample $C_f$-DC where it was not possible to observe the lamellar structure in the

314    section, which appeared in a foam-like state. This structure was restored after the metal insertion, in sample

315    Fe-$C_f$-DC, or alkaline cross-linking, in sample $CC_f$-DC. A clustering of the layers was observed after Fe(III) and

316    V(III) treatment of the $CC_f$-DC. This clustering disappeared after EDTA treatment in sample Fe-$CC_f$-DC (EDTA-

317    Fe-$CC_f$-DC) but not in sample V-$CC_f$-DC (EDTA-V-$CC_f$-DC).

318    As observed in Figure 2 the overall macro-structure of the squid pen was conserved along all the synthetic

319    steps.

320
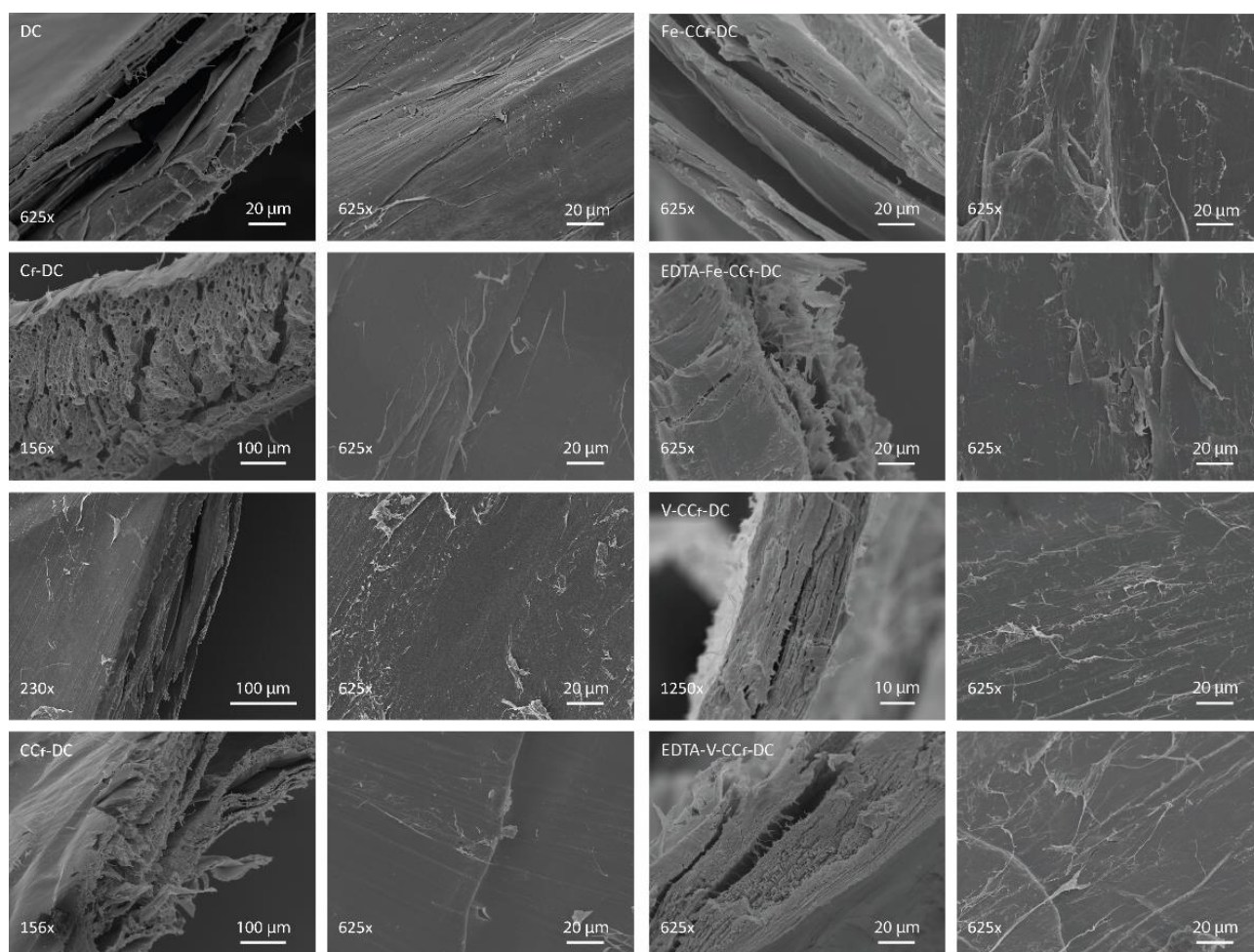
**Figure 6.** SEM images of the matrices synthetizes. For each specimen is reported, on the left, an image of a longitudinal section showing the lamellar structure of the chitinous matrix and, on the right, an image of the sample surface.

## 4. DISCUSSION

The emulation of the complex hierarchical structures produced by the organism is the main goal of biomimetic and bioinspired syntheses. The achievement of this goal has involved the research activity of a plethora of scientists. Although many biomimetic materials have been produced, the faithful reproduction of the evolutionary evolved hierarchical structure of natural materials has been rarely, if ever, achieved. Approaching this research, we realized this difficulty and decided to change the synthetic approach. We used as matrix a hierarchical natural material, not obtainable in laboratory and with the complexity of the variability typical of the natural materials. In it, we added a level of complexity by chemical functionalization. Accordingly, this work produced a family of chitin-based materials from the squid pen, in which the structure of the chitin matrix is preserved and catechol functionalities bioinspired from mussel's byssus thread have been added.

337 The catechol functionalization has been reported for chitosan gels, although in several cases was named

338 chitin functionalization despite the fact that chitin does not form gels in water.(Guo et al., 2015; Kim et al.,

339 2015; Kim, Ryu, Lee, & Lee, 2013; Qiao et al., 2014; Ryu et al., 2011; J. Xu et al., 2015; Zvarec et al., 2013) No

340 work has been reported on actual chitin (with a high DA), or on a chitin hierarchically organized material.

341 Filippidi et al. used also a synthetic approach inspired by mussel byssus, incorporating sacrificial, reversible

342 catechol-Fe(III) cross-links into loosely cross-linked epoxy network.(Filippidi et al., 2017) In this case, a

343 hierarchical structure was missing in the epoxy network.

344 The functionalization with catechols has required an optimization that was governed by the conflicting needs

345 of preserving the native structure of the matrix and maximize its functionalization with catechols. This goal

346 has been achieved as shown by the diffractometric and microscopic investigations and by the observation

347 that the covalently catechol functionalized matrix was able to bind reversibly Fe(III). As consequence of the

348 functionalization, a decrease of the evaluated mechanical properties was observed without a radical change

349 of the crystalline structure of the matrix. This decrease in the mechanical parameters was predictable

350 considering that the specimens were tested hydrated and the functionalized matrix contained over two times

351 the water of the DC. After metal insertion the structurally and crystalline intact matrix obtained, Fe-$C_f$-DC,

352 differed significantly from the $C_f$-DC in E (> 10 times) appearing as a stiffer material, but not able to absorb

353 more energy.

354 The catechols offer also the possibility to generate crosslinking by oxidation with the formation of covalent

355 bonds.(Guo et al., 2015; Pillar, Zhou, & Guzman, 2015) In nature, catechol cross-linked protein networks,

356 such as sclerotized cuticle and byssal threads of the mussel, have been shown to exhibit excellent mechanical

357 properties.(A. Miserez, Schneberk, Sun, W. F., & H. J., 2008; Z. Xu, 2013) According to this information, $C_f$-DC

358 was covalently cross-linked to tune the mechanical resistance in the matrix and induce a slight clustering of

359 the material to favour metal bridges formation. The material obtained showed a marked stiffer behaviour

360 compared to the functionalized matrix having comparable mechanical parameters to that of DC. It is also

361 remarkable that cross-linking reduced variability inside the sample for most mechanical parameters, except

362 for the Young's modulus. The decrease in swelling observed was a validation that a cross-linking occurred.

363 This matrix showed only a slight reversible increase in the stress and work, upon chelation of Fe(III). Thus,

364 the Fe(III) chelation did not add cross-linking useful for the increase of the mechanical performances.

365 The effect of a high level of cross-linking in the matrix was studied in comparison to Fe(III) cross-linking. V(III)

366 was used as oxidant since it has coordination chemistry similar to Fe(III) and the presence of catechol-V(III)

367 complexes can be efficiently detected by Raman spectroscopy.(Montroni et al., 2018) The spectrum excluded

368 the presence of this complex. In addition the UV-Vis spectrum indicated the presence of V(III).(C. Choi et al.,

369 2017; N. H. Choi, Kwon, & Kim, 2013) The V(III) treated matrix did not show significant differences with the

370 $CC_f$-DC except in the swelling, as a hint that the matrix undergoes a further cross-linking. These results show

371    how the exposure to a stronger oxidant did not further increase the mechanical performances of the matrix

372    despite a higher cross-linking occurred. This might be due to the formation of bridges not influencing the

373    mechanical properties.

374    As mentioned, the overall structure was maintained in all the matrices obtained. The XRD pattern was

375    examined for all the matrices and the crystalline structure appeared mostly unaltered. Only a small change

376    on the periodicity associate to the inter-planar distance among chitin planes, the (010) planes, was observed

377    in the Fe(III) cross-linked and oxidized samples. This agreed with the hindrance of these chemical moieties.

378    The microscopic images showed that fibril alignment of the structures was maintained in all the synthetic

379    steps. In agreement with the previous observations after Fe(III) insertion, a reversible clustering of the

380    lamellas was observed, supporting the proved metal-induced cross-linking. The un-expected morphological

381    change observed in the $C_f$-DC, was probably induced by the lyophilisation following highly swelled state, in

382    fact it was not detected in secondary matrices.

383    The experiments performed in this research showed that the improvement of mechanical properties of a

384    hierarchical structured matrix, like the $\beta$-chitin squid pen one, can be achieved using two different strategies,

385    i.e. by formation of coordination bonds with metal ions and by covalent cross-linking. The discussed data

386    show that oxidative treatment with V(III) on alkaline cross-linked matrices does not affect significantly the

387    mechanical properties. This latter observation indicated that the alkaline treatment already saturated the

388    cross-links useful for the improvement of the mechanical properties, as Young modulus of about 10 times.

389    Similarly, in a recent study surface-deacetylated chitin nanofibers that were cross-linked by reaction between

390    quinone and amino groups increased almost 10-fold higher tensile strength.(C. Chen, Li, Yano, & Abe, 2019)

391    The mechanical performances did not change significantly in the alkaline cross-linked matrices after metal

392    ion treatment, although a positive trend was observed. Since the formation of coordination bonds occurs on

393    the same functional groups, only a low improvement is expected. These two cross-link strategies have been

394    widely used by organisms that do not use minerals in their structural tissue. Indeed, while the metal ion

395    coordination bonds is observed for example in the byssus,(Harrington et al., 2010) the catechol cross-linking

396    has been reported in their powerful chitin based mouthparts of the *Dosidicus gigas* (jumbo squids).(Ali

397    Miserez, Li, Waite, & Zok, 2007) Although these studies find inspiration from sclerotization or tanning of

398    chitin in hard tissues of many organisms, they can give hits on the chemical conditions that organisms use to

399    achieve optimal mechanical properties and be of inspiration for synthetic processes. (Cohen, 2010; K. Lee,

400    Prajatelistia, Hwang, & Lee, 2015; A. Miserez et al., 2008; K. Y. Zhu, Merzendorfer, Zhang, Zhang, &

401    Muthukrishnan, 2016)

402

403    5. CONCLUSIONS

We successfully synthetized different advanced materials using a synthetic approach in which a hierarchical natural matrix (i.e. the deproteinized squid pen of *L. vulgaris*) has been functionalized finding inspiration from nature (i.e. byssus).

The functionalized matrices were all able to coordinate Fe(III). The material's mechanical properties were tuneable and/or reversible based on the kind of cross-linking, metal ion chelation (reversible) or oxidative (irreversible), induced on the catechol functional groups. The obtained material, according to the exposed environment, changed from stiffer to softer materials (with E ranging from 30 to 400 MPa and $\sigma_{max}$ from 2.2 to 14 MPa), therefore acting as a stimuli responsive material. Moreover, the two different cross-linking gave materials with different mechanical behaviour. Iron insertion showed mostly an influence on the E (increasing it from 30 to 300 MPa), while oxidation affected all the mechanical parameters (shifting $\varepsilon_{1st\ Failure}$ from 0.12 to 0.07 %, $\sigma_{max}$ from 2.2 to 12 MPa, and E from 30 to 300 MPa). These chemical processes, when differently performed, can allow a diverse customization of the material.

These chelating tuneable matrices might find application and not only in: medicine, as grafts or wound healing materials (being catechols a mucoadhesive enhancing group); water remediation, as chelating matrices; sensors, as metal-responsive materials.

In conclusion, this work shows for the first time that hierarchically organized matrices can be functionalized without altering its multi-scale organization, to get functional materials. This approach could lead to new advanced functional materials combining nature's precisely controlled structure and human's chemistry expertise.

ASSOCIATED CONTENT

**Supporting Information**

Synthetic details; spectroscopic characterization of the materials; results of the microstructural analysis; data on mechanical and physical characterization of the materials.

REFERENCES

Al-Sawalmih, A., Li, C., Siegel, S., Fabritius, H., Yi, S., Raabe, D., … Paris, O. (2008). Microtexture and
chitin/calcite orientation relationship in the mineralized exoskeleton of the american lobster.
*Advanced Functional Materials*, *18*, 3307–3314. https://doi.org/10.1002/adfm.200800520

Anitha, A., Sowmya, S., Kumar, P. T. S., Deepthi, S., Chennazhi, K. P., Ehrlich, H., … Jayakumar, R. (2014).
Chitin and chitosan in selected biomedical applications. *Progress in Polymer Science*, *39*, 1644–1667.
https://doi.org/10.1016/j.progpolymsci.2014.02.008

Asghari, A., Ameri, M., Baraee, B., Rajabi, M., Bakherad, M., & Amoozadeh, A. (2015). Mechanistic
investigation of the electro- oxidation of catechols in the presence of N -methylbenzylamine at room
temperature : synthesis of new quinone derivatives. *Progress in Reaction Kinetics and Mechanism*,
*40*(1), 77–85. https://doi.org/10.3184/146867815X14199390979580

Chabbi, J., Aqil, A., Katir, N., Vertruyen, B., Jerôme, C., Lahcini, M., & El Kadib, A. (2020). Aldehyde-
conjugated chitosan-graphene oxide glucodynamers: Ternary cooperative assembly and controlled
chemical release. *Carbohydrate Polymers*, *230*(June 2019).
https://doi.org/10.1016/j.carbpol.2019.115634

Chen, C., Li, D., Yano, H., & Abe, K. (2019). Bioinspired hydrogels : Quinone crosslinking reaction for chitin
nano fi bers with enhanced mechanical strength via surface deacetylation. *Carbohydrate Polymers*,
*207*(November 2018), 411–417. https://doi.org/10.1016/j.carbpol.2018.12.007

Chen, J., Peng, Q., Peng, X., Han, L., Wang, X., Wang, J., & Zeng, H. (2020). Recent Advances in Mechano-
Responsive Hydrogels for Biomedical Applications. *ACS Applied Polymer Materials*, *2*(3), 1092–1107.
https://doi.org/10.1021/acsapm.0c00019

Chen, W., Shen, X., Hu, Y., Xu, K., Ran, Q., Yu, Y., … Cai, K. (2017). Surface functionalization of titanium
implants with chitosan-catechol conjugate for suppression of ROS-induced cells damage and
improvement of osteogenesis. *Biomaterials*, *114*, 82–96.
https://doi.org/10.1016/j.biomaterials.2016.10.055

Choi, C., Kim, S., Kim, R., Choi, Y., Kim, S., Jung, H. young, … Kim, H. T. (2017). A review of vanadium
electrolytes for vanadium redox flow batteries. *Renewable and Sustainable Energy Reviews*, *69*, 263–
274. https://doi.org/10.1016/j.rser.2016.11.188

Choi, N. H., Kwon, S. K., & Kim, H. (2013). Analysis of the oxidation of the V(II) by dissolved oxygen using UV-
visible spectrophotometry in a vanadium redox flow battery. *Journal of the Electrochemical Society*,
*160*(6), A973–A979. https://doi.org/10.1149/2.145306jes

Cohen, E. (2010). Chitin Biochemistry: Synthesis, Hydrolysis and Inhibition. In *Advances in Insect Physiology*

467       (1st ed., Vol. 38). https://doi.org/10.1016/S0065-2806(10)38005-2

468   Dev, A., Mohan, J. C., Sreeja, V., Tamura, H., Patzke, G. R., Hussain, F., … Jayakumar, R. (2010). Novel

469       carboxymethyl chitin nanoparticles for cancer drug delivery applications. *Carbohydrate Polymers*, *79*,

470       1073–1079. https://doi.org/10.1016/j.carbpol.2009.10.038

471   Eder, M., Amini, S., & Fratzl, P. (2018). Biological composites—complex structures for functional diversity.

472       *Science*, *362*(6414), 543–547. https://doi.org/10.1126/science.aat8297

473   Ehrlich, H., Simon, P., Carrillo-cabrera, W., Bazhenov, V. V, Botting, J. P., Ilan, M., … Paasch, S. (2010).

474       *Insights into Chemistry of Biological Materials : Newly Discovered Silica-Aragonite-Chitin*

475       *Biocomposites in Demosponges*. (9), 1462–1471. https://doi.org/10.1021/cm9026607

476   Fernandez, J. G., & Ingber, D. E. (2013). Bioinspired chitinous material solutions for environmental

477       sustainability and medicine. *Advanced Functional Materials*, *23*, 4454–4466.

478       https://doi.org/10.1002/adfm.201300053

479   Filippidi, E., Cristiani, T. R., Eisenbach, C. D., Waite, J. H., Israelachvili, J. N., Ahn, B. K., & Valentine, M. T.

480       (2017). Toughening elastomers using mussel- inspired iron-catechol complexes. *Science*, *358*, 502–

481       505.

482   Ghiradella, H., & Radigan, W. (n.d.). Development of Butterfly Scales. *J. Morph.*, *150*, 279–298.

483   Ghiradella, Helen. (1994). Structure of butterfly scales: Patterning in an insect cuticle. *Microscopy Research*

484       *and Technique*, *27*, 429–438. https://doi.org/10.1002/jemt.1070270509

485   Guo, Z., Ni, K., Wei, D., & Ren, Y. (2015). Fe $^{3+}$ -induced oxidation and coordination cross-linking in catechol–

486       chitosan hydrogels under acidic pH conditions. *RSC Adv.*, *5*(47), 37377–37384.

487       https://doi.org/10.1039/C5RA03851K

488   Harmoudi, H. El, Gaini, L. El, Daoudi, E., Rhazi, M., Boughaleb, Y., Mhammedi, M. A. El, … Bakasse, M.

489       (2014). Removal of 2,4-D from aqueous solutions by adsorption processes using two biopolymers :

490       chitin and chitosan and their optical properties. *Optical Materials*, *36*, 1471–1477.

491   Harrington, M. J., Masic, A., Holten-andersen, N., Waite, J. H., & Fratzl, P. (2010). Iron-Clad Fibers : A Metal-

492       Based Biological Strategy for Hard Flexible Coatings. *Science*, *328*, 216–221.

493   Heux, L., Brugnerotto, J., Desbriéres, J., Versali, M. F., & Rinaudo, M. (2000). Solid State NMR for

494       Determination of Degree of Acetylation of Chitin and Chitosan. *Biomacromolecules*, *1*, 746–751.

495       https://doi.org/10.1021/bm000070y

496   Holland, B. T., Blanford, C. F., Do, T., & Stein, A. (1999). Synthesis of highly ordered, three-dimensional,

497       macroporous structures of amorphous or crystalline inorganic oxides, phosphates, and hybrid

composites. *Chemistry of Materials*, *11*(3), 795–805. https://doi.org/10.1021/cm980666g

Hunt, S., & El Sherief, A. (1990). A periodic structure in the "pen" chitin of the squid Loligo vulgaris. *Tissue and Cell*, *22*(2), 191–197. https://doi.org/10.1016/0040-8166(90)90021-Z

Hwang, D. S., Harrington, M. J., Lu, Q., Masic, A., Zeng, H., & Waite, J. H. (2012). Mussel foot protein-1 (mcfp-1) interaction with titania surfaces(). *Journal of Materials Chemistry*, *22*(31), 15530–15533. https://doi.org/10.1039/C2JM32439C

Ianiro, A., Giosia, M., Fermani, S., Samorì, C., Barbalinardo, M., Valle, F., … Falini, G. (2014). Customizing Properties of β-Chitin in Squid Pen (Gladius) by Chemical Treatments. *Marine Drugs*, *12*, 5979–5992. https://doi.org/10.3390/md12125979

Ifuku, S., Ikuta, A., Egusa, M., Kaminaka, H., Izawa, H., Morimoto, M., & Saimoto, H. (2013). Preparation of high-strength transparent chitosan film reinforced with surface-deacetylated chitin nanofibers. *Carbohydrate Polymers*, *98*, 1198–1202. https://doi.org/10.1016/j.carbpol.2013.07.033

Kaya, M., Mujtaba, M., Ehrlich, H., Salaberria, A. M., Baran, T., Amemiya, C. T., … Labidi, J. (2017). On chemistry of γ-chitin. *Carbohydrate Polymers*, *176*, 177–186. https://doi.org/10.1016/j.carbpol.2017.08.076

Kennedy, W. R., Dubey, N., Navarro, X., Wendelschafer-Crabb, G., Ceballos, D., & Tranquillo, R. T. (1999). Magnetically Aligned Collagen Gel Filling a Collagen Nerve Guide Improves Peripheral Nerve Regeneration. *Experimental Neurology*, *158*, 290–300. https://doi.org/10.1006/exnr.1999.7111

Kim, K., Kim, K., Hyun, J., & Lee, H. (2015). Chitosan-catechol : A polymer with long-lasting mucoadhesive properties. *Biomaterials*, *52*, 161–170.

Kim, K., Ryu, J. H., Lee, D. Y., & Lee, H. (2013). Bio-inspired catechol conjugation converts water-insoluble chitosan into a highly water-soluble, adhesive chitosan derivative for hydrogels and LbL assembly. *Biomaterials Science*, *1*, 783–790. https://doi.org/10.1039/c3bm00004d

Kinoshita, S., Yoshika, S., Fujii, Y., & Okamoto, N. (2002). Photophysics of Structural Color in the Morpho Butterflies Shuichi. *Forma*, *17*(1), 103–121.

Kurita, K. (2001). Controlled functionalization of the polysaccharide chitin. *Prog. Polym. Sci.*, *26*, 1921–1971.

Lee, H., Dellatore, S. M., Miller, W. M., & Messersmith, P. B. (2007). Mussel-Inspired Surface Chemistry for Multifunctional Coatings. *Science*, *318*, 426–430. https://doi.org/10.1017/CBO9781107415324.004

Lee, K., Prajatelistia, E., Hwang, D. S., & Lee, H. (2015). Role of Dopamine Chemistry in the Formation of Mechanically Strong Mandibles of Grasshoppers. *Chemistry of Materials*, *27*(19), 6478–6481. https://doi.org/10.1021/acs.chemmater.5b01680

529 Li, L., Smitthipong, W., & Zeng, H. (2015). Mussel-inspired hydrogels for biomedical and environmental
530   applications. *Polymer Chemistry*, *6*, 353–358. https://doi.org/10.1039/C4PY01415D

531 Li, Y., Wen, J., Qin, M., Cao, Y., & Wang, W. (2017). Single-Molecule Mechanics of Catechol-Iron
532   Coordination Bonds. *ACS Biomater. Sci. Eng.*, *3*(6), 979–989.
533   https://doi.org/10.1021/acsbiomaterials.7b00186

534 Macquarrie, D. J., & Hardy, J. J. E. (2005). Applications of functionalized chitosan in catalysis. *Industrial and*
535   *Engineering Chemistry Research*, *44*, 8499–8520. https://doi.org/10.1021/ie050007v

536 Martin, L., Wilson, C. G., Koosha, F., Tetley, L., Gray, A. I., Senel, S., & Uchegbu, I. F. (2002). The release of
537   model macromolecules may be controlled by the hydrophobicity of palmitoyl glycol chitosan
538   hydrogels. *Journal of Controlled Release*, *80*, 87–100. https://doi.org/10.1016/S0168-3659(02)00005-6

539 Meyers, M. A., Lin, A. Y. M., Seki, Y., Chen, P., Kad, B. K., & Bodde, S. (2006). Structural Biological
540   Composites : An Overview. *JOM*, *58*, 35–41.

541 Mi, F. L., Shyu, S. S., Chen, C. T., & Lai, J. Y. (2002). Adsorption of indomethacin onto chemically modified
542   chitosan beads. *Polymer*, *43*, 757–765. https://doi.org/10.1016/S0032-3861(01)00580-8

543 Miserez, A., Schneberk, T., Sun, C., W. F., Z., & H. J., W. (2008). The Transition from Stiff to Compliant
544   Materials in Squid Beaks. *Science*, *319*, 1816–1819.

545 Miserez, Ali, Li, Y., Waite, J. H., & Zok, F. (2007). Jumbo squid beaks: Inspiration for design of robust organic
546   composites. *Acta Biomaterialia*, *3*(1), 139–149. https://doi.org/10.1016/j.actbio.2006.09.004

547 Montroni, D., Fermani, S., Morellato, K., Torri, G., Naggi, A., Cristofolini, L., & Falini, G. (2019). β-Chitin
548   samples with similar microfibril arrangement change mechanical properties varying the degree of
549   acetylation. *Carbohydrate Polymers*, *207*, 26–33. https://doi.org/10.1016/j.carbpol.2018.11.069

550 Montroni, D., Marzec, B., Valle, F., Nudelman, F., & Falini, G. (2019). β-Chitin Nanofibril Self-Assembly in
551   Aqueous Environments. *Biomacromolecules*, *20*(6), 2421–2429.
552   https://doi.org/10.1021/acs.biomac.9b00481

553 Montroni, D., Piccinetti, C., Fermani, S., Calvaresi, M., Harrington, M. J., & Falini, G. (2017). Exploitation of
554   mussel byssus mariculture waste as a water remediation material. *RSC Advances*, *7*, 36605–36611.
555   https://doi.org/10.1039/c7ra06664c

556 Montroni, D., Sparla, F., Fermani, S., & Falini, G. (2020). Influence of proteins on mechanical properties of a
557   natural chitin-protein composite. *Acta Biomaterialia*. https://doi.org/10.1016/j.actbio.2020.04.039

558 Montroni, D., Valle, F., Rapino, S., Fermani, S., Calvaresi, M., Harrington, M. J., & Falini, G. (2018).
559   Functional Biocompatible Matrices from Mussel Byssus Waste. *ACS Biomaterials Science and*

Engineering, 4, 57–65. https://doi.org/10.1021/acsbiomaterials.7b00743

Montroni, D., Zhang, X., Leonard, J., Kaya, M., Amemiya, C., Falini, G., & Rolandi, M. (2019). Structural characterization of the buccal mass of Ariolimax californicus (Gastropoda; Stylommatophora). PLoS ONE, 14(8), e0212249.

Muzzarelli, R. A. (2013). Chitin. Elsevier.

Nicklisch, S. C. T., & Waite, J. H. (2012). Mini-review: The role of redox in Dopa-mediated marine adhesion. Biofouling, 28(8), 865–877. https://doi.org/10.1080/08927014.2012.719023

Pillai, C. K. S., Paul, W., & Sharma, C. P. (2009). Chitin and chitosan polymers: Chemistry, solubility and fiber formation. Progress in Polymer Science, 34(7), 641–678. https://doi.org/10.1016/j.progpolymsci.2009.04.001

Pillar, E. A., Zhou, R., & Guzman, M. I. (2015). Heterogeneous Oxidation of Catechol. J. Phys. Chem., 119, 10349–10359. https://doi.org/10.1021/acs.jpca.5b07914

Qiao, H., Sun, M., Su, Z., Xie, Y., Chen, M., Zong, L., … Ping, Q. (2014). Kidney-specific drug delivery system for renal fibrosis based on coordination-driven assembly of catechol-derived chitosan. Biomaterials, 35, 7157–7171. https://doi.org/10.1016/j.biomaterials.2014.04.106

Rathke, T. D., & Hudson, S. M. (1994). Review of Chitin and Chitosan as Fiber and Film Formers. Journal of Macromolecular Science , Part C, 34(3), 374–437.

Ravi Kumar, M. N. . (2000). A review of chitin and chitosan applications. Reactive and Functional Polymers, 46(1), 1–27. https://doi.org/10.1016/S1381-5148(00)00038-9

Ross, S. M. (2003). Peirce's criterion for the elimination of suspect experimental data. Journal of Engineering Technology, 20(2), 38–41.

Ryu, J. H., Jo, S., Koh, M. Y., & Lee, H. (2014). Bio-inspired, water-soluble to insoluble self-conversion for flexible, biocompatible, transparent, catecholamine polysaccharide thin films. Advanced Functional Materials, 24, 7709–7716. https://doi.org/10.1002/adfm.201402250

Ryu, J. H., Lee, Y., Kong, W. H., Kim, T. G., Park, T. G., & Lee, H. (2011). Catechol-Functionalized Chitosan / Pluronic Hydrogels for Tissue Adhesives and Hemostatic Materials †. 2653–2659.

Sashiwa, H., & Aiba, S. I. (2004). Chemically modified chitin and chitosan as biomaterials. Progress in Polymer Science, 29, 887–908. https://doi.org/10.1016/j.progpolymsci.2004.04.001

Seto, J., Ma, Y., Davis, S. A., Meldrum, F., Gourrier, A., Kim, Y. Y., … Cölfen, H. (2012). Structure-property relationships of a biological mesocrystal in the adult sea urchin spine. Proceedings of the National

590    *Academy of Sciences of the United States of America*, *109*(10), 3699–3704.

591    https://doi.org/10.1073/pnas.1109243109

592    Shaala, L. A., Asfour, H. Z., Youssef, D. T. A., ̇Żółtowska-Aksamitowska, S., Wysokowski, M., Tsurkan, M., …

593    Ehrlich, H. (2019). New Source of 3D Chitin Scaffolds : The Red Sea Demosponge Pseudoceratina

594    arabica (Pseudoceratinidae, Verongiida). *Marine Drugs*, *17*, 92–109.

595    https://doi.org/10.3390/md17020092

596    Shams, M. I., Ifuku, S., Nogi, M., Oku, T., & Yano, H. (2011). Fabrication of optically transparent chitin

597    nanocomposites. *Appl Phys A*, *102*, 325–331. https://doi.org/10.1007/s00339-010-5969-5

598    Singh, A., Dutta, P. K., Kumar, H., Kureel, A. K., & Rai, A. K. (2018). Synthesis of chitin-glucan-aldehyde-

599    quercetin conjugate and evaluation of anticancer and antioxidant activities. *Carbohydrate Polymers*,

600    *193*(February), 99–107. https://doi.org/10.1016/j.carbpol.2018.03.092

601    Tsai, C. C., Payne, G. F., & Shen, J. (2018). Exploring pH-Responsive, Switchable Crosslinking Mechanisms for

602    Programming Reconfigurable Hydrogels Based on Aminopolysaccharides. *Chemistry of Materials*,

603    *30*(23), 8597–8605. https://doi.org/10.1021/acs.chemmater.8b03753

604    Weaver, J. C., Milliron, G. W., Miserez, A., Evans-lutterodt, K., Herrera, S., Gallana, I., … Kisailus, D. (2012).

605    The Stomatopod Dactyl Club : A Formidable Damage-Tolerant Biological Hammer. *Science*, *336*(June),

606    1275–1280. https://doi.org/10.1126/science.1218764

607    Wysokowski, M., Petrenko, I., Stelling, A. L., Stawski, D., Jesionowski, T., & Ehrlich, H. (2015). Poriferan

608    chitin as a versatile template for extreme biomimetics. *Polymers*, *7*, 235–265.

609    https://doi.org/10.3390/polym7020235

610    Xu, H., Nishida, J., Wu, H., Kobayashi, M., Otsuka, H., & Takahara, A. (2012). Competition between

611    Oxidation and Coordination in Cross-Linking of Polystyrene Copolymer Containing Catechol Groups.

612    *ACS Macro Lett.*, *1*, 457–460. https://doi.org/10.1021/mz200217d

613    Xu, J., Strandman, S., Zhu, J. X. X., Barralet, J., & Cerruti, M. (2015). Genipin-crosslinked catechol-chitosan

614    mucoadhesive hydrogels for buccal drug delivery. *Biomaterials*, *37*, 395–404.

615    https://doi.org/10.1016/j.biomaterials.2014.10.024

616    Xu, Z. (2013). Mechanics of metal-catecholate complexes: the roles of coordination state and metal types.

617    *Scientific Reports*, *3*, 2914. https://doi.org/10.1038/srep02914

618    Yang, S. S., Chen, Y. di, Zhang, Y., Zhou, H. M., Ji, X. Y., He, L., … Wu, W. M. (2019). A novel clean production

619    approach to utilize crop waste residues as co-diet for mealworm (Tenebrio molitor) biomass

620    production with biochar as byproduct for heavy metal removal. *Environmental Pollution*, *252*, 1142–

621        1153. https://doi.org/10.1016/j.envpol.2019.06.028

622    Zhu, K., Tu, H., Yang, P., Qiu, C., Zhang, D., Lu, A., … Zhang, L. (2019). Mechanically Strong Chitin Fibers with

623        Nanofibril Structure, Biocompatibility, and Biodegradability. *Chemistry of Materials*, *31*(6), 2078–2087.

624        https://doi.org/10.1021/acs.chemmater.8b05183

625    Zhu, K. Y., Merzendorfer, H., Zhang, W., Zhang, J., & Muthukrishnan, S. (2016). Biosynthesis, Turnover, and

626        Functions of Chitin in Insects. *Annual Review of Entomology*, *61*, 177–196.

627        https://doi.org/10.1146/annurev-ento-010715-023933

628    Zvarec, O., Purushotham, S., Masic, A., Ramanujan, R. V, & Miserez, A. (2013). *Catechol-Functionalized*

629        *Chitosan/Iron Oxide Nanoparticle Composite Inspired by Mussel Thread Coating and Squid Beak*

630        *Interfacial Chemistry*.

631

632